A piezoelectric cantilever-beam energy harvester (PCEH) with a rectangular hole in the metal substrate

Yuzhong Xiong[1] · Fang Song[1,2] · Xinghuan Leng[2]

Abstract

In order to improve the energy conversion performance of a piezoelectric cantilever-beam energy harvester (PCEH), a novel PCEH is developed and designed according to the typical PCEH. Its middle layer is a metal substrate with a rectangular hole. The mathematical model of the PCEH is analyzed, and the mathematical expressions of the eigenfrequency, the displacement of the proof mass and the output voltage and power are derived. In order to verify the validity of the model, the eigenfrequency and frequency domain are analyzed by using COMSOL and Matlab, and the influence of frequency, load resistance and acceleration on voltage and power is studied. Finally, the experimental verification was carried out to further confirm. The results show that the first-order eigenfrequency of the novel PCEH is 43.7 Hz, the optimal output power is 10.69 mW. Therefore, the novel PCEH has a lower frequency, a wider frequency band, and higher output voltage and power, and improves energy conversion performance.

1 Introduction

With the development of low-energy, low-power and independent working systems such as micromechanical technology, embedded devices and wireless sensor networks, the demand for independent power supply becomes more and more urgent (Mitcheson et al. 2004a). Nowadays, most devices are powered by the traditional way of a battery, which has a series of problems such as short life and frequent replacement. To solve these problems, people carry out long-term research, using energy in the environment into electricity. Therefore, energy harvesting technology has become one of the hot spots in current research.

Energy harvesting is a technology that converts the energy existing in the surrounding environment into electric energy and stores it in energy storage devices. The energy sources may come from available but unutilized energy in nature, including sound energy, thermal energy, kinetic energy, light energy, wind energy, tidal energy and so on (Manjunath et al. 2012; Feng et al. 2013). Vibration is ubiquitous in the living environment. Cars, trains, subways, airplanes, and other equipment all vibrate when they operate. And thus, mechanical vibration energy is a universal energy source. Therefore, the research of energy harvesting mainly focuses on mechanical vibration energy acquisition.

Mechanical vibration energy acquisition mainly uses vibration energy harvesters to convert mechanical energy in the environment into electrical energy. Vibration energy harvesters are classified as electromagnetic (Hussam et al. 2009; Chiu and Tseng 2008; Mitcheson et al. 2004b; Daniel et al. 2009), electrostatic (Williams et al. 2001; Williams and Yates 1996; Shearwood and Yates 1997), piezoelectric (Mikio et al. 1996; Umeda et al. 1997; Antaki et al. 1995; Kim et al. 2004; Li et al. 2018a) and magnetostrictive (Flatau and Staley 2005; Huang et al. 2003; Bayrashev et al. 2004; Wang and Yuan 2008). Piezoelectric energy harvesters convert mechanical vibrational energy into electrical energy through the positive piezoelectric effect of piezoelectric materials. Compared with

✉ Fang Song
songfang2005@163.com

Yuzhong Xiong
362996309@qq.com

Xinghuan Leng
327367621@qq.com

[1] School of Mechanical and Automotive Engineering, Shanghai University of Engineering Science, 333 Longteng Road, Songjiang District, 201620 Shanghai, China

[2] Engineering Training Center, Shanghai University of Engineering Science, 333 Longteng Road, Songjiang District, 201620 Shanghai, China

other energy harvesters, piezoelectric energy harvesters have many advantages such as simple structure, high energy density, free from electromagnetic interference, small size, low cost and so on. Therefore, the research on piezoelectric energy harvesters is the most extensive.

With the continuous research on piezoelectric energy harvesters, piezoelectric energy harvesting technology has been greatly improved. Huicong Liu et al. (2011) proposed a piezoelectric energy harvesting cantilever beam integrated with silicon proof mass material. It can obtain energy from low-frequency ambient vibration. Six series–parallel PZT modes were studied to optimize the output power. Salem and Othman (2015) proposed a MEMS-based array energy harvester model and simulated it under ambient vibration excitation using the Coventorware method. This model can achieve a lower frequency response, resulting in greater voltage and power. Usharani et al. (2017) designed a piezoelectric cantilever beam energy harvester with a step section. The harvester, which the cantilever beam is piezoelectric-patched, achieved higher power in a broadband operating frequency. Li et al. (2018a) designed a wearable energy harvester that converts low-frequency motion into high-frequency motion to improve energy conversion. In order to improve the energy conversion performance of a PCEH, this paper will introduce a PCEH with a rectangular hole in the metal substrate. We know that the power of PZT is generated by deformation, and the larger the deformation, the more power is generated. Therefore, I tried to make the PZT produce a larger deformation by changing the structure of the PCEH. Eventually, I designed a substrate with a rectangular hole to make the strain around the rectangular hole larger and to make the PCEH more strained and more power generated. In addition, this structure also reduces the structural volume and overall quality of the device. The next section will introduce the theoretical model of the energy harvester and perform geometric analysis and theoretical analysis. In the third section, the numerical solution and simulation analysis will be carried out, and the results will be analyzed and compared to verify the validity of the model. The fourth and fifth sections will conduct experiments, and analyze and discuss the experimental results to further validate the results of the third section. The sixth section is the conclusion of this paper.

2 Theoretical model of PCEH

2.1 Geometric structure

Figure 1a shows the structure of a typical PCEH, which is composed of a fixed base, a cantilever beam, and a proof mass. One end of the cantilever beam is fixed in the base
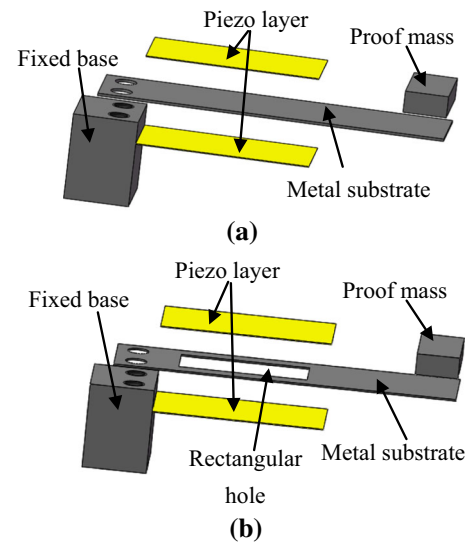

Fig. 1 Structure diagram of PCEH **a** without a rectangular hole, **b** with a rectangular hole
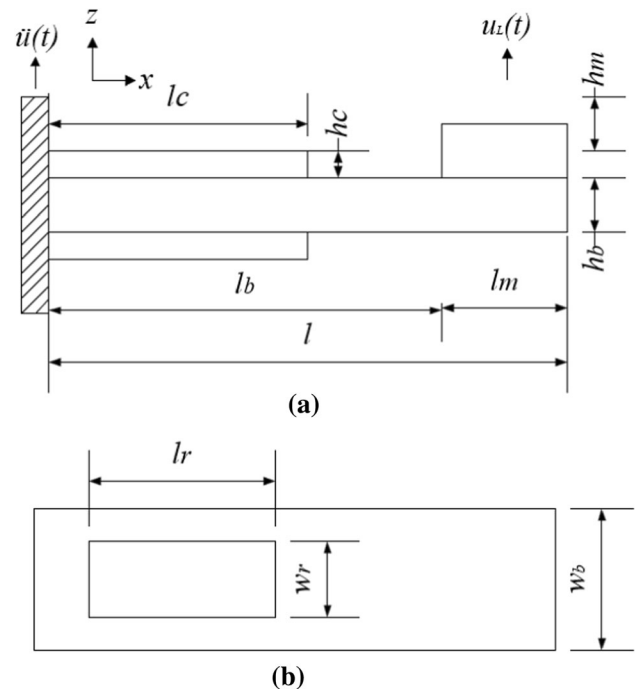

Fig. 2 Simplified structure diagram. The picture **a** is a front view of the novel PCEH, the figure **b** shows a metal substrate with a rectangular hole

and the other end is free. The upper and lower layers of the cantilever beam are piezoelectric layers, and the middle layer is a metal substrate. The proof mass is placed at the free end of the cantilever beam.

Figure 1b shows the PCEH with a rectangular hole in the metal substrate. The difference with Fig. 1a is that the metal substrate has a rectangular hole structure.

2.2 Theoretical analysis

The performance of PCEH is related to the structural parameters of the device. The performance of the device we care about mainly includes eigenfrequency, output voltage, and power. In order to improve the output performance of the device, the structural parameters of the energy harvester which affect the output performance are optimized, and the relationship between the structural parameters and the output performance is obtained. Note that we neglect in this analysis the dielectric and piezoelectric losses which can occur in the structure.

In this paper, the geometric structure shown in Fig. 1b is simplified, and the structure diagram is shown in Fig. 2. In the diagram, the x-direction is the axial direction of the cantilever beam, and the displacement of the proof mass at the free end is $u_L(t)$ under the action of the external basic acceleration with the size of $\ddot{u}(t)$. The total length of the cantilever beam is l, and the horizontal distance between the fixed base and the proof mass is l_b. The length of the proof mass is l_m, the thickness is h_m, and the mass is m. In the middle layer of the cantilever beam, the length of the metal substrate is l, the thickness is h_b, and the length of the rectangular hole is l_r. The length of the upper and lower piezoelectric layers is l_c, the thickness is h_c. Except for the rectangular hole with the width of w_r, the other all structures are w_b.

As can be seen from the diagram, the piezoelectric cantilever beam is composed of the upper and lower piezoelectric layers and the metal substrate located in the middle layer. The stiffness of the entire piezoelectric cantilever beam can be equivalent to that of the piezoelectric cantilever which all layers are seen as piezoelectric layers. Therefore, the overall equivalent stiffness of the piezoelectric cantilever beam can be expressed as:

$$EcI = EbIb + 2EcIc \tag{1}$$

Hence Eq. (1) can be written as:

$$I = 2Ic + \frac{Eb}{Ec}Ib \tag{2}$$

Where Ec and Eb represent Young's modulus of the piezoelectric layer and metal substrate respectively, Ic and Ib represent the moment of inertia of the piezoelectric layer and the substrate layer respectively.

Then the bending moment of the PCEH is solved. Since the bending moment of the piezoelectric cantilever beam is different at different positions along the x-axis when it vibrates, we can use the section method to solve the problem. According to the moment balance principle of mechanics, the bending moment of piezoelectric cantilever beam at x from the fixed base can be obtained as:

$$M(x) = Fm(t)\left(l - \frac{1}{2}lm - x\right) \tag{3}$$

Where $Fm(t) = m\ddot{u}_L(t)$.

Therefore, the average stress of the piezoelectric layer on the cross-section of the piezoelectric cantilever beam can be expressed as:

$$\sigma(x) = \frac{M(x)h_{cb}}{I} \tag{4}$$

Where $h_{cb} = \frac{hc+hb}{2}$, is the distance between the neutral layer of the piezoelectric layer and the neutral layer of the metal substrate.

According to the piezoelectric layer with the length of l_c, the Eq. (4) is integrated and averaged to obtain the average effective stress formula of the piezoelectric layer, as shown in Eq. (5).

$$\sigma = \frac{1}{lc}\int_0^{lc}\frac{M(x)h_{cb}}{I}dx \tag{5}$$

Then, substituting Eq. (3) into Eq. (5):

$$\sigma = Fm(t)\frac{(2l - lc - lm)h_{cb}}{2I} \tag{6}$$

Equation (6) shows the relationship between the stress of the piezoelectric layer and the force of the proof mass. This relationship is expressed by the coefficient $\lambda 1$:

$$\lambda 1 = \frac{(2l - lc - lm)h_{cb}}{2I} \tag{7}$$

The standard equation for the Euler–Bernoulli beam is expressed as (Zhang et al. 2017):

$$\frac{d^2u(x)}{dx^2} = \frac{M(x)}{EcI} \tag{8}$$

Where $u(x)$ is the relative displacement in the vertical direction at x from the fixed base.

Substituting Eq. (3) into Eq. (8), and then integrating it twice. If $\dot{u}(0) = u(0) = 0, x = l - lm$, the following equation can be obtained:

$$u = \frac{F_m(t)(l - lm)^2}{12EcI}(4l - lm) \tag{9}$$

The stress–strain formula can be written as:

$$\sigma = Ec\varepsilon \tag{10}$$

In combination with Eqs. (6), (9) and (10), the relationship, expressed by the coefficient $\lambda 2$, between the strain of piezoelectric cantilever beam and the relative displacement of the proof mass in the vertical direction can be obtained:

$$\lambda 2 = \frac{\varepsilon}{u} = \frac{(l-l_m)^2(4l-l_m)}{6(2l-lc-l_m)h_{cb}} \quad (11)$$

So, by combining Eqs. (6), (7), (10) and (11), the equivalent spring coefficient of piezoelectric cantilever beam can be obtained:

$$\lambda = \frac{Ec}{\lambda_1\lambda_2} \quad (12)$$

Regarding the proof mass at the free end as a small point, the eigenfrequency of the cantilever beam can be expressed as (Yi et al. 2002):

$$fn = \frac{\eta'^2_n}{2\pi}\sqrt{\frac{\lambda}{me+m}} \quad (13)$$

Where n is the mode index, $\eta'^2_n = \eta^2_n\sqrt{\frac{0.236}{3}}$, η_n is the frequency coefficient. The equivalent mass of piezoelectric cantilever beam is $me = 0.236(2mc+mb)$, where m_c and m_b are the mass of the piezoelectric layer and the mass of metal substrate respectively.

Therefore, by substituting Eq. (12) into Eq. (13), the eigenfrequency can be expressed as:

$$fn = \frac{\eta^2_n}{2\pi}\sqrt{\frac{0.236Ec}{3[0.236(2mc+mb)+m]\lambda_1\lambda_2}} \quad (14)$$

The electromechanical coupled dynamic equation and Kirchhoff's law of the circuit loop can be used to establish an equivalent circuit model as (Li et al. 2018b):

$$m\ddot{u}_L(t) + D\dot{u}_L(t) + \lambda u_L(t) + \theta V(t) = m\ddot{u}(t) \quad (15)$$

$$Cce\dot{V}(t) + \frac{V(t)}{R} - \theta\dot{u}_L(t) = 0 \quad (16)$$

Where $u_L(t)$, D, θ, Cce and R are the displacement, damping coefficient, piezoelectric coupling coefficient, the capacitance of the piezoelectric layer and load resistance, respectively. D and λ can be obtained by $D = 2\zeta_m\omega_n m$ and $\lambda = \frac{Ec}{\lambda_1\lambda_2} = \omega^2_n m$ respectively, where ζ_m and ω_n are the mechanical damping ratio and natural frequency of the system respectively. Cce can be obtained by $C_{ce} = \frac{k\varepsilon^s_{33}w_b l_c}{2h_c}$, where $k = 1$ represents two piezoelectric layers in series; $k = 2$ represents two piezoelectric layers in parallel.

The Laplace transform is performed for Eqs. (15) and (16), and then replace the variable s with $j\omega$ to get the expression of voltage and power:

$$|V| = \frac{\frac{2\omega E_c d_{31} h_c}{k\varepsilon^s_{33}\lambda_2}O_{in}}{\sqrt{\left[\frac{1}{RC_{ce}}\omega^2_n - \left(\frac{1}{RC_{ce}}+2\zeta_m\omega_n\right)\omega^2\right]^2 + \omega^2\left[\omega^2_n(1+\gamma^2)+\frac{2\zeta_m\omega_n}{RC_{ce}}-\omega^2\right]^2}} \quad (17)$$

$$P = \frac{|V|^2}{R} \quad (18)$$

where $\gamma^2 = \frac{d^2_{31}E_c}{\varepsilon^s_{33}}$, O_{in} is the Laplace transform of the input acceleration. The analysis of Eq. (17), (18) shows that the maximum output voltage and power of the device are inversely proportional to eigenfrequency, proportional to acceleration and piezoelectric strain constant, and related to its structural parameters.

3 Numerical calculation and simulation analysis

This section briefly introduces the details of finite element simulation analysis, including the geometric model, loading and boundary conditions, etc. Moreover, the numerical calculation of the analysis model in the second section is carried out, and the comparison between the calculation results and the simulation results verifies the reliability of the analysis model.

3.1 Geometric model

In order to compare the power generation performance of the PCEH with or without a rectangular hole, the finite element simulation analysis of the two types of energy harvesters was carried out. Figure 1a and b are their structures, established by Solidworks, respectively. The same materials are used for each part of the two types of PCEHs. The proof mass and fixed base are made of structural steel, the metal substrate is made of aluminum, and the piezoelectric layers are made of PZT-5H. Table 1 shows the dimensional parameters of the two energy harvesters, and Table 2 shows the performance parameters of various materials.

3.2 Modal analysis and results

Modal analysis was performed by COMSOL Multiphysics. In the select physics tree of COMSOL, the eigenfrequency study is selected. A fixed constraint boundary condition is applied to the bottom of the fixed base of the energy harvester, and then conventional meshing is performed.

Table 1 Dimensional parameters of the two PCEHs

Name	Length (mm)	Width (mm)	Thickness (mm)
Metal substrate	80	20	0.6
Rectangular hole	30	12	0.6
Piezo layer	40	20	0.2
Proof mass	10	20	5
Fixed base	15	20	20

Table 2 Material performance parameters

	PZT-5H	Aluminum	Structural steel
Density (kg/m³)	7500	2700	7850
Young's modulus (GPa)	61	70	200
$d_{31}(10^{-10}$ m/V)	2.74		
$\varepsilon_{33}^s(10^{-8}$ F/m)	3.009		
$\varepsilon_0(10^{-12}$ F/m)	8.85		
Poisson's ratio	0.289	0.33	0.30

Table 3 First six eigenfrequencies of the two PCEHs

Modal	The typical (Hz)	The novel (Hz)
1	53.475	50.831
2	340.98	330.33
3	460.68	460. 37
4	1120.9	1056.3
5	1251.2	1248.5
6	1908.7	1765.8

Through the simulation, the 6 mode eigenfrequencies of the two types of energy harvesters are obtained, as shown in Table 3.

According to Eq. (14) and the various parameters of PCEH, the first-order eigenfrequency of the two types of energy harvesters are obtained by Matlab, which are 52.78 Hz and 48.83 Hz, respectively. Compared with the first-order eigenfrequency in Table 3, the error is 1.3% and 3.9%, respectively.

It can be seen that the eigenfrequencies of the novel PCEH are lower than those of the typical in Table 3. Therefore, the novel PCEH has a wider frequency range and can exhibit better power generation performance under low-frequency vibration environment.

3.3 Frequency domain analysis

3.3.1 Frequency response: voltage and power

In COMSOL, frequency domain study is added, and then frequency domain analysis is carried out for two kinds of PCEHs. The parameters are set in the global definition: acceleration and load resistance. Where acceleration is acc = 1 g, g is the unit and represents the acceleration constant of gravity, the load resistance is R_load = 12 kΩ, and the mechanical damping ratio is 0.01. The relationship between frequency and voltage & power of the two types of PCEHs is measured under the conditions that a unit-body load of size -solid.rho*g_const*acc is applied to the
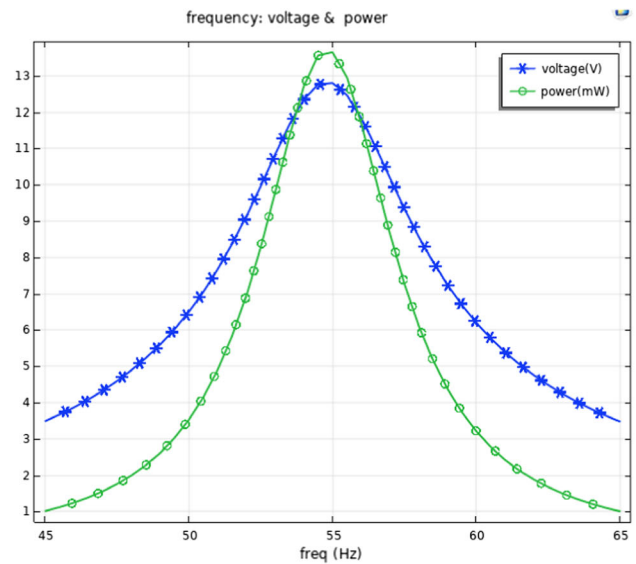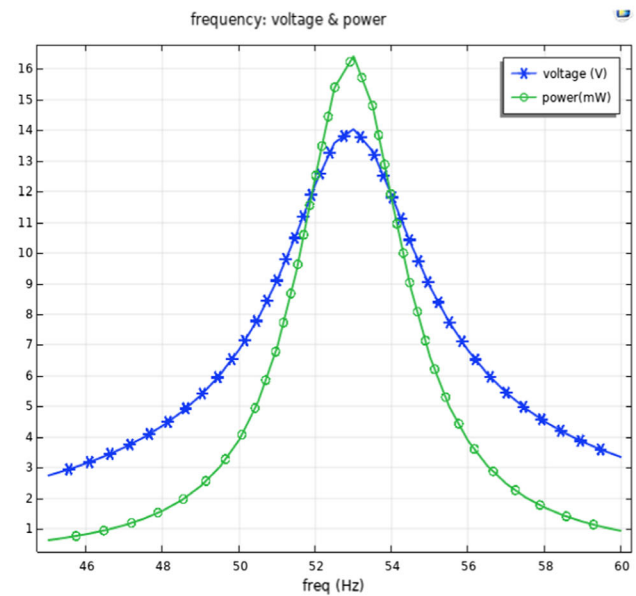
Fig. 3 PCEHs power harvested (in mW) and the peak voltage induced across the piezoelectric bimorph (in V) vs. excitation frequency. **a** the typical and **b** the novel

PCEHs, a fixed constraint is applied to the bottom of the fixed base, and the load resistance is R_load in the circuit. Figure 3a and b show the relationship graphs.

It can be seen from Fig. 3a that the typical PCEH reaches a peak voltage of 12.8 V at 54.5 Hz, and that the output power is 13.65 mW. It can be seen from Fig. 3b that the PCEH, with a rectangular hole, reaches a peak voltage of 14.04 V at 53 Hz, and that the output power is 16.43 mW. By comparison, it can be found that the output voltage and power of the novel PCEH are higher than the

typical under the excitation of the first-order eigenfrequency.

In order to verify the reliability of the analytical model in Sect. 2, the numerical results were obtained by calculations for Eqs. (17), (18), and the results are shown in Fig. 4a and b. As can be seen from the figure, the peak voltage and power of the typical are 14.7 V and 18.03 mW, and the novel are 16.69 V and 23.23 mW, respectively.

According to Figs. 3, 4, Table 3 and the first-order eigenfrequency obtained by calculation, it is found that the numerical calculation results are basically consistent with the simulation results. Therefore, the correctness of the second section of the model has been verified. Next, only the simulation analysis will be performed, and no numerical calculation will be performed.
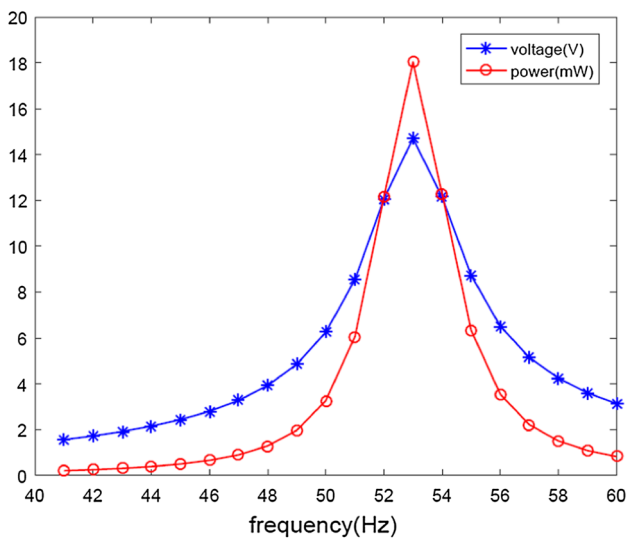

(a)
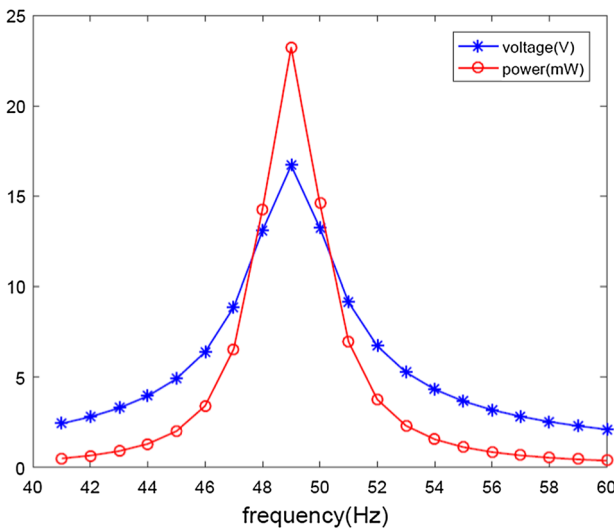
(b)

Fig. 4 The output power and voltage obtained by numerical calculation under different frequencies. **a** The typical and **b** the novel

3.3.2 Load dependence: voltage and power

R_load = 10^range(2,0.1,6) is typed in the Study Extensions of the frequency domain study. The acceleration is 1 g oscillating at 54.5 Hz and 53 Hz respectively. The relationship between frequency and voltage and power of the two types of PCEHs can be obtained by changes in load resistance.

According to Fig. 5a, when the excitation frequency of the typical PCEH is 54.5 Hz, the voltage increases with the increase of the load, and finally reaches the maximum
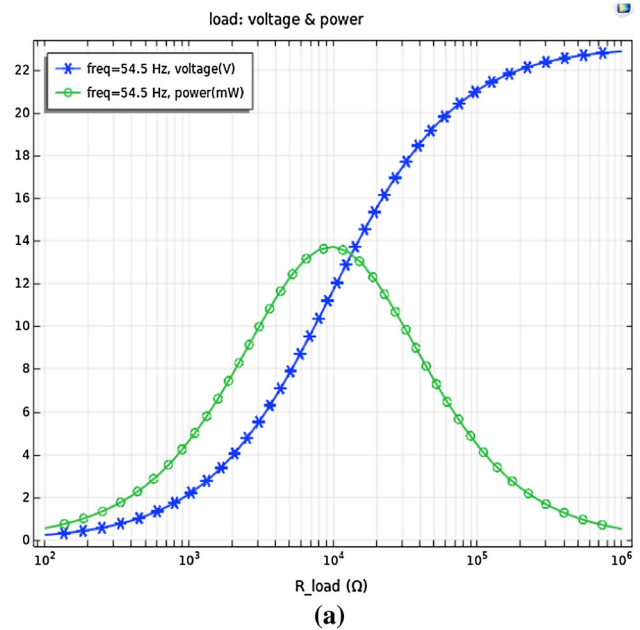
(a)
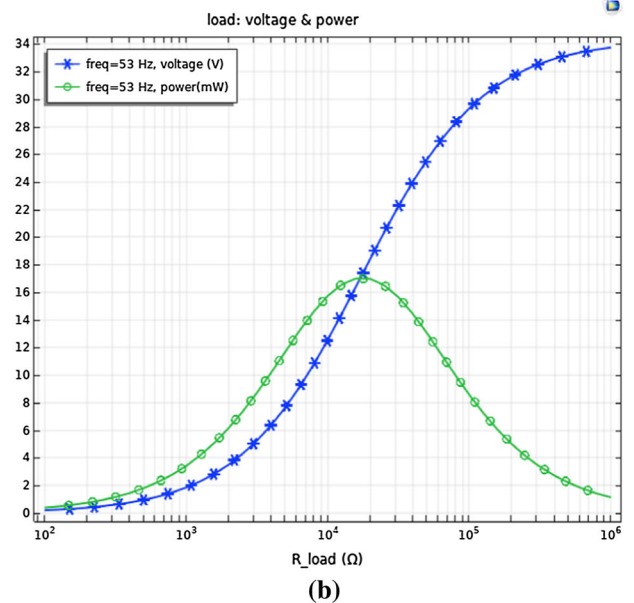
(b)

Fig. 5 Energy harvested from the device as a function of the electrical load resistance at an acceleration of 1 g oscillating at **a** 54.5 Hz and **b** 53 Hz, respectively. **a** The typical and **b** the novel

value, that is, the open-circuit voltage. It can be seen from the figure that the open-circuit voltage is 22.86 V. The power increases first and then decreases with the increase of the load. The maximum power is 13.71 mW. According to Fig. 5b, when the excitation frequency of the novel PCEH is 53 Hz, the voltage also increases with the increase of the applied load until the maximum value is reached. The open-circuit voltage value is 33.75 V. Similarly, the change of power is the same as that of the typical PCEH, the maximum power is 17 mW. The comparison found that the open-circuit voltage of the novel is 1.48 times that of the typical under the excitation of the respective first-order eigenfrequency. The power is 3.29 mW higher than the typical.

3.3.3 Acceleration dependence: voltage and power

acc = range (0.25,0.25,1.25) is typed in the Study Extensions of the frequency domain study. The applied load resistance is the optimal impedance of the two PCEHs. Figure 5 shows that the optimal impedance is 10 kΩ and 15.85 kΩ, respectively. The relationship between frequency and voltage & power of the two types of PCEHs can be obtained by change of acceleration.

According to Fig. 6a and b, both voltage and power increase as the acceleration increases. It is apparent from the figures that the novel PCEH grows much faster than the typical one. Thus, the novel PCEH has better piezoelectric properties.

4 Experiment

The PCEH was fabricated according to the dimensions and materials of Tables 1 and 2. The PZT-5H was attached to the substrate using SINWE 6529 epoxy conductive adhesive and then cured for 24 h. The conductive adhesive is a two-component epoxy adhesive with copper powder as a conductive material and has the characteristics of high bonding strength, good electrical conductivity, low electrical resistance, high and low temperature resistance. For the novel PCEH, the substrate has a rectangular hole that needs to be machined. The laser cutting is used to process the holes. The laser cutting machine needs to be continuously debugged, and a series of parameters, such as air pressure, cutting speed, cutting height and cutting frequency, need to be adjusted to ensure the smooth cutting.

The prepared energy harvester is subjected to experimental testing. Figure 7 shows a block diagram of the testing system. The system consists of a signal generator (SCM205), power amplifier (HEA-200C), shaker (HEV-200), accelerometer (SILICON DESIGNS 2220-010), data acquisition card (DAQ card) (SILICON DESIGNS), PC,
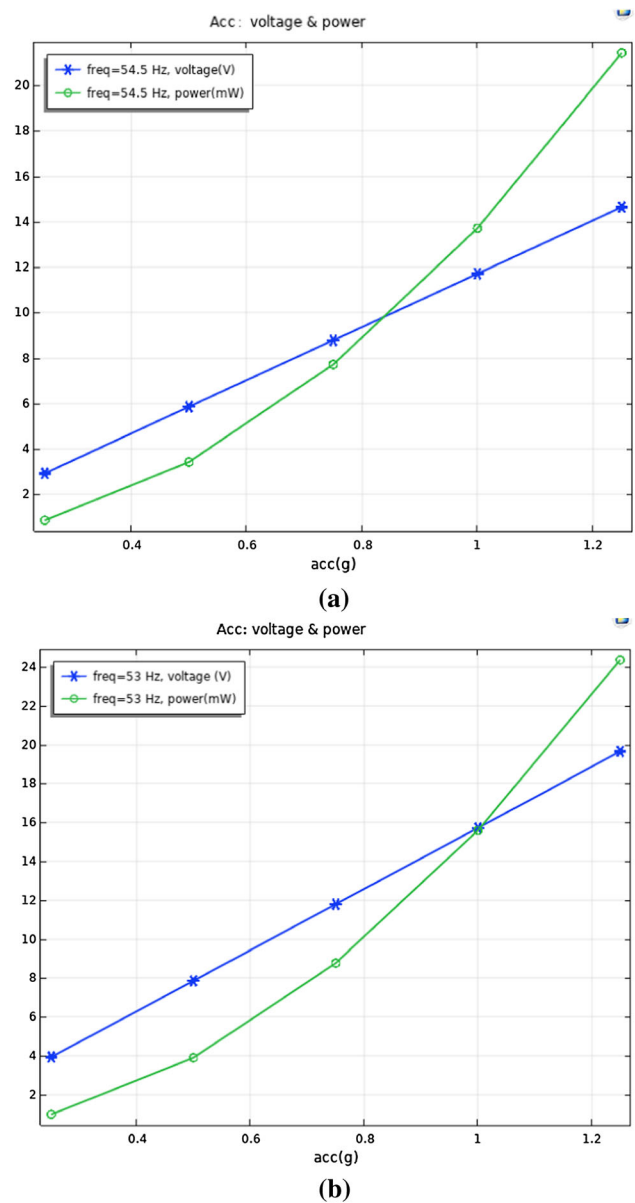
(a)

(b)

Fig. 6 Energy harvested from the device as a func-tion of the acceleration at a load resistance of **a** 10 kΩ and **b** 15.85 kΩ oscillating at **a** 54.5 Hz and **b** 53 Hz, respectively. **a** the typical and **b** the novel

load and oscilloscope (Tektronix MDO3012). The experimental figure of the entire test system is shown in Fig. 8.

During the test, the prepared PCEH is fixed on the shaker, and the accelerometer is fixed on the fixed end of the energy harvester. Then the signal generator generates a sine wave signal with a certain frequency, which is amplified by the power amplifier to drive the shaker to simulate the actual environment vibration. The vibration acceleration is monitored by the accelerometer, DAQ card, and PC in real time, and controlled by adjusting the power
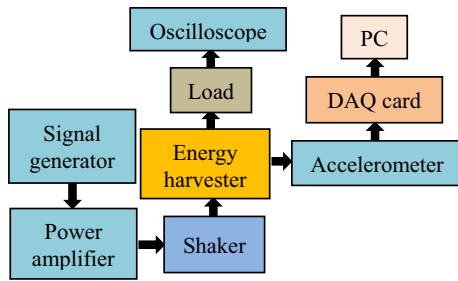
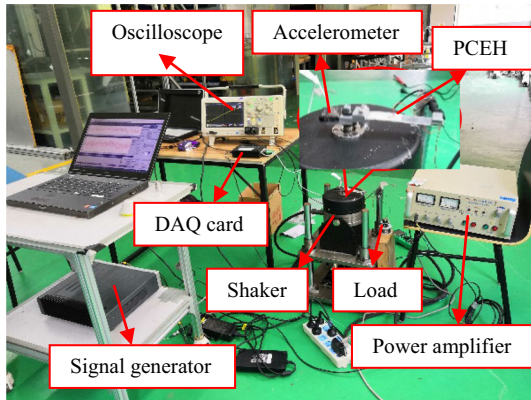**Fig. 7** Block diagram of the testing system

Fig. 8 Test system of PCEH

amplifier as needed. The output electrical signal is recorded by an oscilloscope.

5 Results and discussion

Experimental tests were performed with reference to simulation conditions. The output voltage and power under different frequency, load, and acceleration conditions are obtained through experiments. Figure 9 shows the output voltage and power vs. frequency, load, and acceleration. In the experiment, the acceleration is 1 g, the load resistance is 12 kΩ, and the single-frequency excitation vibration method is used for testing. The instantaneous output peak value of PCEH at different frequencies is taken as the result at this frequency, and finally, the result shown in Fig. 9a is obtained. As can be seen from the results, the first-order eigenfrequency of the typical PCEH is 48.6 Hz, and the novel is 43.7 Hz. The maximum output voltage and power of the typical are 9.26 V and 7.15 mW, and the novel are 11.02 V and 10.11 mW, respectively. Then, set the frequency to the first-order eigenfrequency obtained by experiment, change the load resistance, and obtain the peak output as the result, and the result shown in Fig. 9b is
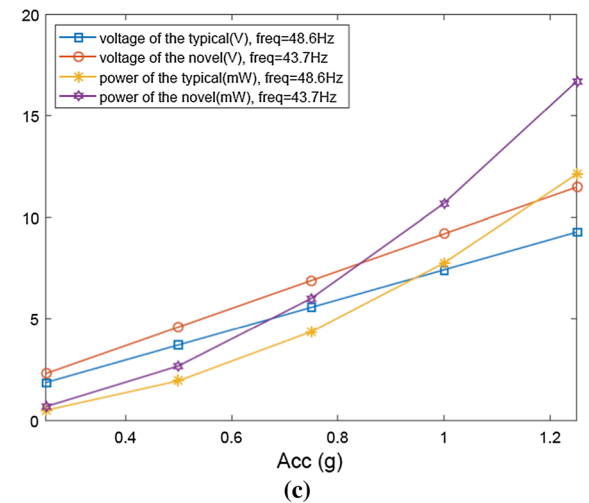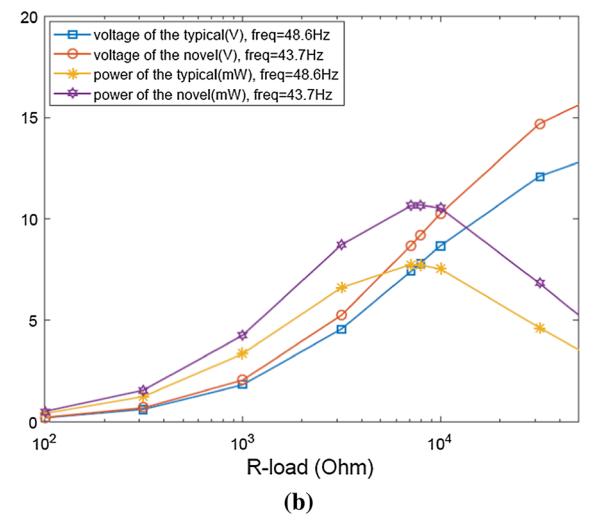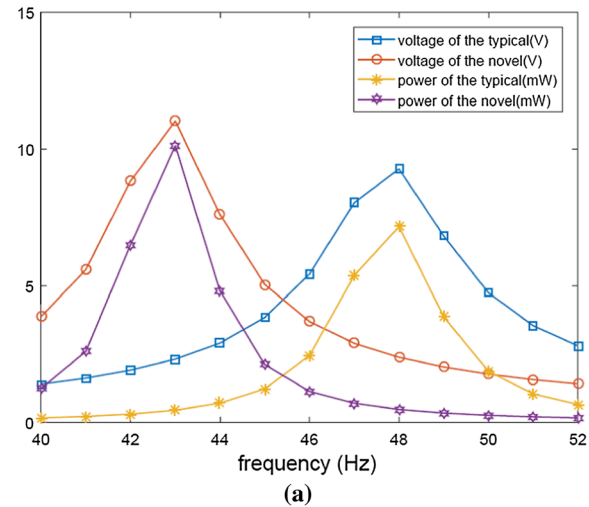

Fig. 9 The output voltage and power of experimental results for two types of PCEHs. **a** Frequency response, **b** load dependence, **c** acceleration dependence

obtained. The results show that the optimal load and output power of the typical are 7.1 kΩ and 8.70 mW, and the novel are 7.9 kΩ and 10.69 mW, respectively. Finally, under the conditions of optimal load and first-order eigenfrequency, the acceleration is changed to obtain the result shown in Fig. 9c.

Comparing the experimental results with the results of numerical calculation and simulation, we can see that the output performance of the experimental results is slightly lower than that of the calculation and simulation. This is mainly because some factors such as dielectric loss, coupling loss, and transmission loss are not considered in numerical calculation and simulation. But these factors are actually there. In addition, it also includes the fact that the manufactured PCEH is not exactly the same as the ideal PCEH. Therefore, there are gaps between actual results obtained by experiments and simulation and numerical calculations. The experimental results are within the error range and are acceptable. Through experiments, the results have in good agreement with the numerical analysis and simulation results, further verify the validity of the model, and indicate that the novel PCEH has better power generation performance.

6 Conclusion

In this paper, a novel PCEH is proposed by optimizing the structural design of a typical PCEH. The intermediate metal substrate of the novel energy harvester has a rectangular hole. The effects of the hole on power generation performance were studied by mathematical model analysis and finite element analysis, and verified by experiments. The results show that the PCEH, with a rectangular hole, has a lower eigenfrequency and can work better under low-frequency environment excitation. It achieves high output power at a low resonant frequency of 43.7 Hz. When the excitation frequency matches the eigenfrequency and the novel PCEH is connected to the optimal resistance load, the output power is as high as 10.69 mW. It is higher than the typical. Overall, this study achieved higher energy output with simple structural optimization, driving the advancement and development of micro energy technology and energy harvesting technology.

References

Antaki JF, Bertocci GE et al (1995) Gait-powered autologous battery charging system for artificial organs. ASAIO J 41:588–595

Bayrashev A, Robbins WP, Ziaie B (2004) Low frequency wireless powering of micro-systems using piezoelectric-magnetostric-tive laminate composite. Sens Actuators A 114(2–3):244–249

Chiu Y, Tseng VFG (2008) A capacitive vibration-to-electricity energy converter with integrated mechanical switches. J Micromech Microeng 18:104004

Daniel H, Bernd F et al (2009) Fabrication, characterization and modeling of electrostatic micro-generators. J Micromech Microeng 19:094001

Flatau AB, Staley ME (2005) Characterization of energy harvesting potential of Terfenol-D and Galfenol. Proc SPIE 5764:630–640

Feng L, Luo J, Shi G et al (2013) Frequency allocation for versatile occupancy of spectrum in wireless sensor networks. In: Proceedings of the 14th ACM Conference Mobile Ad Hoc 25(6):39-48

Hussam K, Daniel H, Bernd F et al (2009) A micro capacitive vibration energy harvester for low power electronics. Power MEMS. https://www.researchgate.net/publication/267998601_A_MICRO_CAPACITIVE_VIBRATION_ENERGY_HARVESTER_FOR_LOW_POWER_ELECTRONICS

Huang J, O'Handley RC, Bono D (2003) New high-sensitivity hybrid magnetostrictive/electroactive magnetic field sensors. Proc SPIE 5050:229–237

Kim HW, Batra A, Priya S et al (2004) Energy harvesting using a piezoelectric "cymbal" transducer in dynamic environment. Jpn J Appl Phys 43:6178–6183

Li TL, Mohamed MA, Yahya I et al (2018a) Comparison of piezoelectric energy harvesting performance using silicon and graphene cantilever beam. Microsyst Technol 24(9):3783–3789

Li KL, He QH, Wang JC et al (2018b) Wearable energy harvesters generating electricity from low-frequency human limb movement. Microsyst Nanoeng 4:24

Liu HC, Quan CG, Cho JT et al (2011) A MEMS-based piezoelectric cantilever patterned with PZT thin film array for harvesting energy from low frequency vibrations. Phys Procedia 19:129–133

Manjunath D, Chan MC, Ananda AL (2012) Indriya: a low-cost, 3D wireless sensor network testbed. Dev Netw Communities 90(4):302–316

Mikio U, Kentaro N, Sadayuki U (1996) Analysis of the transformation of mecha-nical impact energy to electric energy using piezoelectric vibrator. Jpn J Appl Phys 35:3267–3273

Mitcheson PD, Green TC, Yeatman EM et al (2004a) Architectures for vibration-driven micropower generators. JMEMS 3(13):429–440

Mitcheson PD, Miao P, Stark BH et al (2004b) MEMS electrostatic micropower generator for low frequency operation. Sens Actuators A 115:523–529

Salem S, Othman S (2015) Micro-electro-mechanical system (MEMS)-based piezo-electric energy harvester for ambient vibrations. Procedia-Soc Behav Sci 195:2353–2362

Shearwood C, Yates RB (1997) Development of an electromagnetic micro-generator. Electron Lett 33(22):1883–1884

Umeda M, Nakamura K, Ueha S (1997) Energy storage characteristics of a piezogenerator using impact induced vibration. Jpn J Appl Phys 36:3146–3151

Usharani R, Uma G, Umapathy M et al (2017) A new piezoelectric-patched cantilever beam with a step section for high performance of energy harvesting. Sens Actuators A 265:47–61

Wang L, Yuan FG (2008) Vibration energy harvesting by magnetostrictive material. Smart Mater Struct 17(4):45009–45014

Williams CB, Yates RB (1996) Analysis of a micro-electric generator for Microsystems. Sens Actuators A 52(1–3):8–11

Williams CB, Shearwood C, Harradine MA et al (2001) Development of an electro-magnettic micro-generator. IEE Proc-Circuits Devices Syst 148(6):337–342

Yi JW, Shih WY, Shih WH (2002) Effect of length, width, and mode on the mass detection sensitivity of piezoelectric unimorph cantilevers. J Appl Phys 91:1680–1686

Zhang GY, Gao SQ, Liu HP, Niu SH (2017) A low frequency piezoelectric energy harvester with trapezoidal cantilever beam: theory and experiment. Microsyst Technol 23(8):3457–3466